Measurement of the enhanced evanescent fields of integrated waveguides for optical near-field sensing

Julia Hahn,[1,*] Christian E. Rüter,[2] Frank Fecher,[1] Jürgen Petter,[1] Detlef Kip,[2] and Theo Tschudi[1]

[1]Institute of Applied Physics, Technische Universität Darmstadt, Hochschulstrasse 6, 64289 Darmstadt, Germany

[2]Institute of Physics and Physical Technology, Clausthal University of Technology, Leibnizstrasse 4, 38678 Clausthal-Zellerfeld, Germany

*Corresponding author: julia.hahn@physik.tu-darmstadt.de

Received 3 January 2008; revised 2 April 2008; accepted 4 April 2008; posted 4 April 2008 (Doc. ID 91131); published 28 April 2008

The sensitivity of an integrated optical sensing device can be enhanced by coating it with a high refractive index layer, while both incoupled intensity and spatial resolution are maintained. The potential for enhanced sensing is demonstrated using titanium indiffused waveguiding structures in $LiNbO_3$ coated with a TiO_2 film. To the best of our knowledge, it could be measured for the first time that the outcoupled intensity at the surface was enhanced by a factor of 12–15 while keeping the penetration depth of the evanescent field constant of the order of only a few tens of nanometers. The evanescent fields of the guided modes were measured and characterized with a scanning near-field optical microscope and are in accordance with the numerical simulations.

OCIS codes: 130.3730, 180.4243, 230.3120, 310.2785.

1. Introduction

The interaction of evanescent fields of light propagating in waveguiding structures with a covering medium has been used in numerous applications, including sensing devices [1–3], tunable optical filters [4,5], and the excitation of fluorescent dyes in thin layers with high spatial resolution [6]. Because of the variety of application possibilities in many scientific fields it has become inevitable to properly design the spatial shape and propagation constants of guided modes, which also influences their evanescent parts and allows for tailoring them for specific applications.

In the general case of a mode propagating in a waveguiding structure, the term evanescent field refers to the part of the electric field E that penetrates into the optically thinner medium [7,8]. Along the waveguide normal, it is described by an exponentially decaying function

$$E = E_0 \exp(-z/d_p), \tag{1}$$

where E_0 is the electrical field strength at the interface, z is the distance from the interface in the optically thinner medium, and d_p is the penetration depth. The penetration depth d_p is characteristic for a waveguiding structure. It depends on the distribution of the refractive indices of the waveguide and the surrounding media (and, therefore, the geometry), and the properties of the guided light, e.g., wavelength and polarization.

For some applications, such as the optical monitoring of biological and chemical processes at boundary layers (i.e., at the interface of a waveguide structure), it is essential to concentrate the light intensity to very short distances above the interface. In evanescent field illumination the penetration depth d_p is the determining value for the thickness of the illuminated

0003-6935/08/132357-04$15.00/0

layer [9]. It is desirable to keep it as small as possible, otherwise spatial resolution in the z direction will deteriorate [10]. At the same time, an enhancement of the field strength E_0 at the interface without changing the penetration depth d_p is favorable, since then higher intensities are available for interaction processes in the boundary layer of the covering medium. It has been shown that such an increase of the proportion of the guided mode field that penetrates into the covering medium can be achieved by coating the waveguide with a thin high-index metal oxide film [11].

In this work we present both theoretical calculations and experimental measurements of the evanescent field distribution of a single-mode waveguiding channel in lithium niobate ($LiNbO_3$). This material has good electro-optic performances, and the fabrication of low-loss waveguides is well established [12]. Furthermore, $LiNbO_3$ has a rather high refractive index, which leads to a low penetration depth of the evanescent field of the order of only a few tens of nanometers into the covering medium, which makes this material highly appropriate for evanescent field sensors. Both uncoated waveguide channels as well as channels coated with a thin high-index TiO_2 film are fabricated. For the latter case, an enhancement of the evanescent field strength by more than 1 order of magnitude is found using a scanning near-field optical microscope (SNOM).

2. Sample Fabrication

For the experiments coherent green light with a wavelength of $\lambda = 532\,\text{nm}$ is used. The crystal sample was cut from an undoped x-cut $LiNbO_3$ wafer of congruently melting composition. It had dimensions of $1\,\text{mm} \times 25\,\text{mm} \times 10\,\text{mm}$ with the z axis pointing along the 10 mm long ferroelectric c axis. The waveguides were prepared by patterning a 10 nm thick titanium layer using standard photolithographic techniques forming $6\,\mu\text{m}$ wide stripes running parallel to the 25 mm long y axis. Subsequently, the stripes were indiffused for 2 h at 1273 K in air. Titanium increases both the ordinary and the extraordinary refractive index of the $LiNbO_3$ substrate. As a result, low-loss single-mode channel waveguides for TE-polarized light of 532 nm wavelength are formed. After waveguide fabrication an 80 nm thick layer of titanium dioxide (TiO_2) was deposited on top of one-half of the channel waveguides by reactive sputtering (thus leaving the other half uncoated for direct comparison). Finally, the endfaces of the crystals were polished and an optical fiber was attached by index-matched ultraviolet light curing adhesive to guarantee reproducibility of the incoupling of light into the waveguide.

3. Numerical Simulations

To calculate the field distribution and the propagation constants of the modes of the isolated single channel waveguide the scalar Helmholtz equation is solved using the finite difference approach. The refractive index profile of the waveguide is obtained by solving the diffusion equation for a depletable source with parameters related to the experimental data given above. The resulting titanium concentration profile is transferred into a refractive index distribution using the method described in [13,14]. The bulk extraordinary refractive index $n_e = 2.2335$ of $LiNbO_3$ for wavelength $\lambda = 532\,\text{nm}$ is taken from [15]. Because of the indiffused titanium the refractive index at the surface is increased by $\Delta n_e = 0.0107$. The index profile along the waveguide normal (z direction) inside the substrate is described by a Gaussian function

$$n_e(z) = n_e + \Delta n_e \exp(-z^2/\sigma^2), \tag{2}$$

with a Gaussian width of $\sigma = 0.6\,\mu\text{m}$. For part of the calculations the high-refractive index layer of TiO_2 is added to the refractive index profile. Since the TiO_2 is present in the form of anatase, a refractive index of 2.40 was used for the numerical simulations [16].

4. Experimental Results

Measurements of the evanescent field intensities were taken by employing a SNOM in collection mode. A tapered glass fiber tip penetrated the evanescent field above the waveguide. The light tunneled the gap between waveguide and fiber and was collected by fiber and guided to a photomultiplier. The tip was attached to a tuning fork and the whole system was mounted to a three-axis piezodriven positioning unit under an angle of $\theta \approx 30°$ as depicted in Fig. 1. This geometry was chosen for stability reasons and to minimize the ablation of the fragile tip. The electrical signal of the damped oscillating tuning fork was used for distance control, which is an established technique in SNOM measurements [17–19]. The position $z = 0$, which defines the direct contact with the surface, was particularly obtained from that signal. Because of the shape of the tip [20] and the performance of the actuators, resolution in the z direction was of the order of $\Delta z = 5\,\text{nm}$, whereas resolution in the x and y directions was of the order of $\Delta x = \Delta y = 0.8\,\mu\text{m}$.

Measurements were performed for both uncoated and TiO_2 coated regions of the channel waveguide. In Fig. 2 the collected intensity is shown in logarithmic scale as a function of height z above the sample surface. Approaching the surface ($z > 0$) the intensity rises exponentially and peaks at the interface

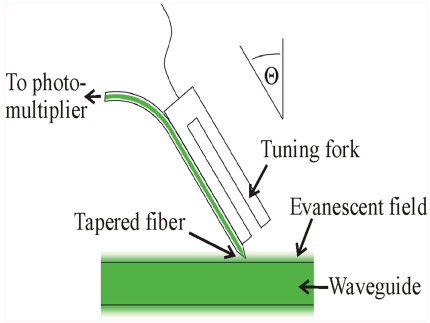

Fig. 1. (Color online) Experimental geometry of the SNOM setup.

($z = 0$). The decrease of the intensity for negative z values in the plot does not refer to positions inside the crystal but can be explained by the fiber tip touching the surface and then bending upward under further pressure.

All measurements were taken at the center (y direction) of the channel waveguides under identical conditions. Therefore, the intensities at the interfaces can be directly compared. The intensity $I_{c,z=0}$ at the interface of coating and air is enhanced by a factor of 12 compared to the value of $I_{u,z=0}$ at the interface of the uncoated sample and air.

From the curves plotted in Fig. 2 an exponential decay was fitted with resulting penetration depths $d_{\mathrm{pi},u} = (43 \pm 13)\,\mathrm{nm}$ and $d_{\mathrm{pi},c} = (57 \pm 8)\,\mathrm{nm}$. With the above described numerical simulations, penetration depths of $d_{\mathrm{pi,sim}} = 21.2\,\mathrm{nm}$ were calculated for both uncoated and coated samples. These measured penetration depths d_{pi} refer to the intensity and are half of the value of the characteristic value d_p, which refers to the field strength as given by Eq. (1).

The measured penetration depths exceed the calculated ones by a factor of 2 in the case of an uncoated waveguide and by a factor of 2.7 in the case of the TiO_2 coated waveguide. This discrepancy and the relatively high error of the measured values were predominantly caused by the relatively round shape of the fiber tip used in the SNOM setup. Despite the loss of resolution, the round shape was preferred to a more rectangular one, since the latter would have decreased the efficiency of the incoupling of the tunneling evanescent field into the fiber. Subsequently, the photon counting efficiency as well as the signal-to-noise ratio of the photomultiplier tube used would have reduced the accuracy of the measurement. This also explains why the deviation of the measured penetration depth in the case of the uncoated area of the waveguide exceeds the one in the coated area, where the intensity signal is higher. Nevertheless, all values for the penetration depths are of the same order of magnitude of a few tens of nanometers.

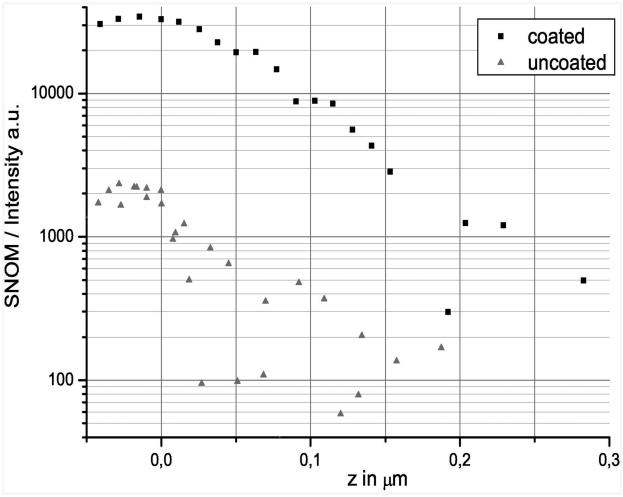

Fig. 2. Height (z) dependence of the evanescent field intensity collected with the SNOM for coated and uncoated regions of the waveguide.

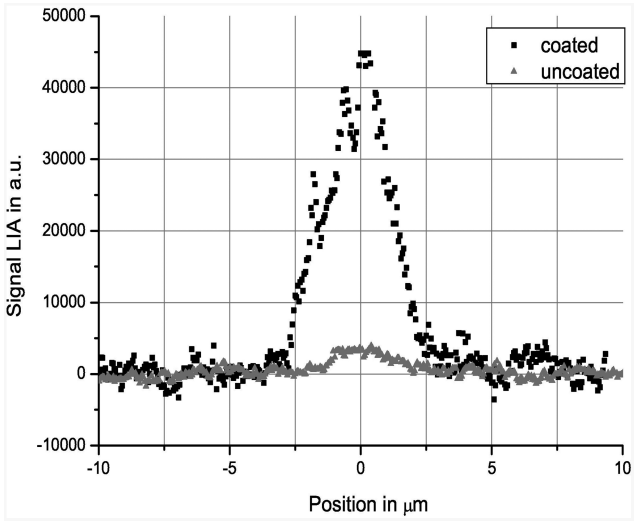

Fig. 3. Lateral (y) scan of the evanescent field intensity in contact with both coated and uncoated regions of the waveguide.

Another experiment was performed to investigate the enhancement of the intensity of the evanescent field by lateral scans of the fiber tip in the y direction at the surface using the tapping mode of the SNOM, again for both uncoated and TiO_2 coated regions of the channels. In Fig. 3 lateral scans for both regions are shown. Again, the intensity of the evanescent field in the coated region is enhanced when compared to the intensity in the uncoated region. For the peaks at the center of the waveguide a ratio of $I_{c,z=0}/I_{u,z=0} = 15$ is found.

A comparison of the measured and calculated intensity distribution at the surface is shown in Fig. 4 for the coated region and in Fig. 5 for the uncoated region. The FWHM values obtained from the simulation (for both regions) are $\mathrm{FWHM_{sim}} = 2.8\,\mu\mathrm{m}$, whereas for the measured curves, we find $\mathrm{FWHM_{measured}} = 2.7 \pm 0.1\,\mu\mathrm{m}$ in both regions. The experimental results are in good accord with the theoretical calculations.

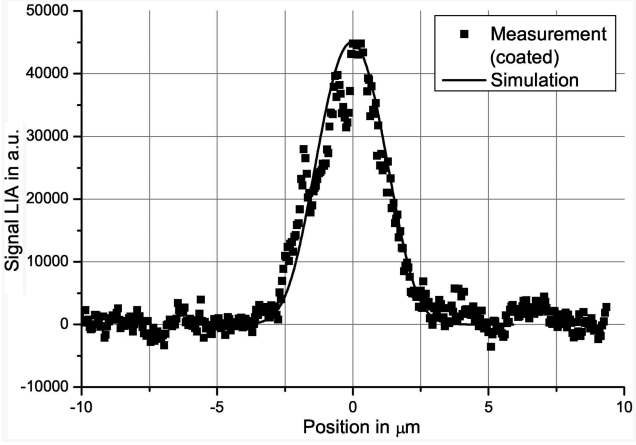

Fig. 4. Measured and calculated intensity distribution in contact with the coated waveguide.

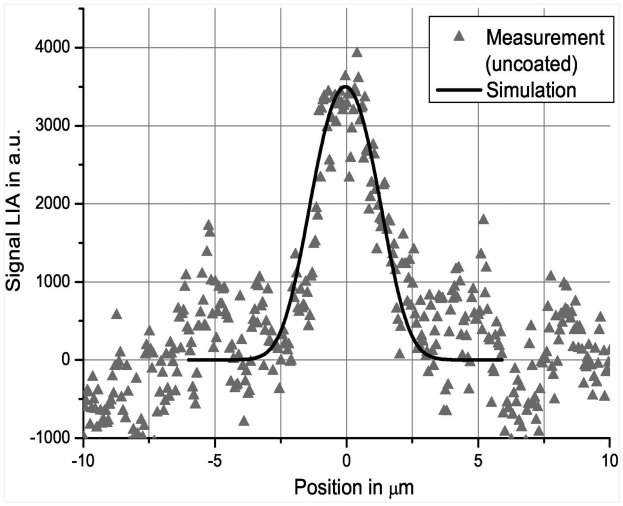

Fig. 5. Measured and calculated intensity distribution in contact with the uncoated waveguide.

5. Discussion and Conclusion

Measurements of the evanescent field intensities of modes guided in titanium indiffused waveguides in $LiNbO_3$ crystals were performed by probing the field with a tapered SNOM fiber tip in scanning mode and the results were compared to numerical simulations. The simulations predict that, in spite of the change in the field distribution inside the waveguide and a subsequent enhancement of the intensity at the interface by 1 order of magnitude, the penetration depth remains unchanged when the waveguide is coated by a thin layer of TiO_2.

The calculated value of the penetration depth and the lateral intensity distribution are in good agreement with existing literature [21,22]. Nevertheless, the measured penetration depths exceed the calculated ones by a factor of 2 in the case of an uncoated waveguide and by a factor of 2.7 in the case of the TiO_2 coated waveguide. For the lateral scan theoretical and experimental curves were in good agreement. It could be shown that by covering the titanium indiffused waveguide in $LiNbO_3$ with an 80 nm thick layer of TiO_2 the intensity of the field at the surface was enhanced by a factor of 12–15.

In conclusion, sensitivity enhancement of an integrated near-field optical device due to enhancement of the proportion of mode intensity guided as an evanescent wave above the waveguide surface has been successfully demonstrated for the first time, while keeping the extremely short penetration depth of the guided light almost unchanged. The presented manipulation and characterization of the field of titanium indiffused waveguides in $LiNbO_3$ by coating them with a TiO_2 layer makes these devices attractive for applications where low penetration depths of the order of a few tens of nanometers with rather high intensities at the surface are required.

References

1. G. Boisdé and A. Harmer, *Chemical and Biochemical Sensing with Optical Fibers and Waveguides* (Artech House, 1996).
2. R. E. Kunz, "Miniature integrated optical modules for chemical and biochemical sensing," Sens. Actuators B **38**, 13–28 (1997).
3. C. R. Lavers, K. Itoh, S. C. Wu, M. Murabayashi, I. Mauchline, G. Stewart, and T. Stout, "Planar optical waveguides for sensing applications," Sens. Actuators B **69**, 85–95 (2000).
4. M. P. Petrov, A. V. Chamrai, A. S. Kozlov, and I. V. Ilichev, "Electrically controlled integrated optical filter," Tech. Phys. Lett. **30**, 120–122 (2004).
5. P. Arora, A. S. Kozlov, I. V. Ilichev, A. V. Chamray, V. M. Petrov, J. Petter, M. P. Petrov, and T. Tschudi, "Synthesis of the transfer function of a spectral Bragg filter using electro-optical phase-shift keying," in *Proceedings of the Conference on Lasers and Electro-Optics* (CLEO, 2007), paper CMG 5.
6. C. R. Taitt, G. P. Anderson, and F. S. Ligler, "Evanescent wave fluorescence biosensors," Biosens. Bioelectron. **20**, 2470–2487 (2005).
7. B. E. A. Saleh and M. C. Teich, *Fundamentals of Photonics* (Wiley, 1991).
8. F. de Fornel, *Evanescent Waves* (Springer, 2001).
9. D. Axelrod, "Cell-substrate contacts illuminated by total internal reflection fluorescence," J. Cell Biol. **89**, 141–145 (1981).
10. M. Oheim, "Quantitative high-resolution fluorescence microscopy using evanescent-wave excitation," Ph.D. dissertation (Universität Göttingen, 1998).
11. G. R. Quigley, R. D. Harris, and J. S. Wilkinson, "Sensitivity enhancement of integrated optical sensors by use of thin high-index films," Appl. Opt. **38**, 6036–6039 (1999).
12. D. Kip, "Photorefractive waveguides in oxide crystals: fabrication, properties, and applications," Appl. Phys. B **67**, 131–150 (1998).
13. J. Hukriede, D. Runde, and D. Kip, "Fabrication and application of holographic Bragg gratings in photorefractive lithium niobate channel waveguides," J. Phys. D **36**, R1–R16 (2003).
14. J. Vollmer, J. P. Nisius, P. Hertel, and E. Krätzig, "Refractive-index profiles of $LiNbO_3$–Ti waveguides," Appl. Phys. A **32**, 125–127 (1983).
15. U. Schlarp and K. Betzler, "Refractive index of lithium niobate as a function of temperature, wavelength and composition: a general fit," Phys. Rev. B **48**, 15613–15620 (1993).
16. P. Löbl, M. Huppertz, and D. Mergel, "Nucleation and growth in TiO_2 films prepared by sputtering and evaporation," Thin Solid Films **251**, 72–79 (1994).
17. K. Karrai and R. D. Grober, "Piezoelectric tip-sample distance control for near field optical microscopes," Appl. Phys. Lett. **66**, 1842 (1995).
18. H. Edwards, L. Taylor, W. Duncan, and A. J. Melmed, "Fast, high-resolution atomic force microscopy using a quartz tuning fork as actuator and sensor," J. Appl. Phys. **82**, 980–984 (1997).
19. D. P. Tsai and Y. Y. Lu, "Tapping-mode tuning fork force sensing for near-field scanning optical microscopy," Appl. Phys. Lett. **73**, 2724–2727 (1998).
20. L. Salomon, F. de Fornel, and J. P. Goudennet, "Sample-tip coupling efficiencies of the photon-scanning tunneling microscope," J. Opt. Soc. Am. A **8**, 2009–2015 (1991).
21. S. Tascu, P. Moretti, S. Kostritskii, and B. Jacquier, "Optical near-field measurements of guided modes in various processed $LiNbO_3$ and $LiTaO_3$ channel waveguides," Opt. Mater. **24**, 297–302 (2003).
22. A. L. Campillo, J. W. P. Hsu, C. A. White, and C. D. W. Jones, "Direct measurement of the guided modes in $LiNbO_3$ waveguides," Appl. Phys. Lett. **80**, 2239–2241 (2002).